J. Fluid Mech. (2000), *vol.* 407, *pp.* 105–122. Printed in the United Kingdom

© 2000 Cambridge University Press

Enhanced dissipation for quasi-geostrophic motion over small-scale topography

By JACQUES VANNESTE

Department of Mathematics and Statistics, University of Edinburgh, James Clerk Maxwell Building, King's Buildings, Mayfield Road, Edinburgh EH9 3JZ, UK

(Received 22 March 1999 and in revised form 7 October 1999)

The effect of a small-scale topography on large-scale, small-amplitude oceanic motion is analysed using a two-dimensional quasi-geostrophic model that includes free-surface and β effects, Ekman friction and viscous (or turbulent) dissipation. The topography is two-dimensional and periodic; its slope is assumed to be much larger than the ratio of the ocean depth to the Earth's radius. An averaged equation of motion is derived for flows with spatial scales that are much larger than the scale of the topography and either (i) much larger than or (ii) comparable to the radius of deformation. Compared to the standard quasi-geostrophic equation, this averaged equation contains an additional dissipative term that results from the interaction between topography and dissipation. In case (i) this term simply represents an additional Ekman friction, whereas in case (ii) it is given by an integral over the history of the large-scale flow. The properties of the additional term are studied in detail. For case (i) in particular, numerical calculations are employed to analyse the dependence of the additional Ekman friction on the structure of the topography and on the strength of the original dissipation mechanisms.

1. Introduction

Sea-floor topography plays an important role in the dynamics of the oceans through a variety of mechanisms. One of these, which is captured in simple quasi-geostrophic models, is the vortex stretching that results from changes in the water depth. Because of the Earth's rotation, it leads to the appearance of a restoring force and associated waves, the topographic Rossby waves (e.g. Pedlosky 1987). Topographic Rossby waves, and more generally Rossby waves supported by both topography and β-effect, have been studied theoretically in detail in various settings (e.g. Rhines 1970*a*, *b*; Rhines & Bretherton 1973; Reznik & Tsybaneva 1999, and references therein).

A question of great practical interest concerns the effect of the smallest scales of the topography: these scales cannot be resolved in numerical simulations, yet they are likely to have a significant influence on the large-scale motion. Theoretical studies are thus crucial to assess the importance and nature of this influence. Most rigorous studies of this type concentrate on the effect of topography on the propagation of Rossby waves; they use the linearized barotropic (or multilayer) quasi-geostrophic equation and employ asymptotic techniques relying on the separation between the scale of the topography and the scale of the motion. Thomson (1975), for instance, studied the weak scattering of Rossby waves that is caused by a shallow random topography (see also Prahalad & Sengupta 1986). More recent work focuses on the (Anderson) localization of Rossby waves, that is, on the existence of localized

https://doi.org/10.1017/S0022112099007430 Published online by Cambridge University Press

free waves (Sengupta, Piterbarg & Reznik 1992; Sengupta 1994) – or similarly the evanescence of forced waves (Klyatskin 1996; Klyatskin, Gryanik & Gurarie 1998) – that results from the randomness of the topography.

These studies have two important features in common: they neglect dissipative effects and consider one-dimensional topographies. Here, by contrast, we are interested in the interactions between topography and dissipation and we consider a two-dimensional topography. We therefore analyse the barotropic quasi-geostrophic equation including Ekman friction and a viscous term that can be regarded as a parameterization of turbulent dissipation. Using a multiple-scale expansion, we derive an averaged (or homogenized) version of this equation valid for motion with a scale much larger than that of the topography. As is detailed in § 2, the scaling is chosen so that the effect of the topography appears at leading order in the averaged equation. This effect is described by an additional dissipative term, which in general depends on the history of the large-scale flow. In the limit of a radius of deformation small compared to the scale of the motion (and of the order of the topography scale), however, it reduces to an additional Ekman friction.

Thus, the interplay between topography and dissipative effects is shown to lead primarily to an enhancement of the dissipation. The physical mechanism behind this enhancement is clear: when interacting with the topography, the large-scale motion generates a weak small-scale flow. Because of its small scale, and despite its small amplitude, this flow is efficiently damped by the Ekman friction and turbulent dissipation; it acts thus as an energy sink for the large-scale motion. This picture appears transparently in the formal derivation of the averaged equation given in § 3.

We analyse in some detail the additional dissipative term, first (i) for small radius of deformation (the long-wave regime, § 4), then (ii) for a radius of deformation of the same order as the scale of the motion (the short-wave regime, § 5). Numerical computations are required to evaluate the coefficients that appear in the averaged equation for a given topography. In case (i), these coefficients are the (constant) components of an Ekman friction tensor. We calculate them for two simple topographies and discuss their asymptotic form in the limit of strong and weak dissipation. In case (ii), by contrast, the coefficients are functions of time and their numerical computation raises several issues going beyond the scope of this paper. We thus restrict our attention to their analytical properties. A few remarks conclude the paper in § 6; they are devoted to the relationship between our study and that of Gama, Vergassola & Frisch (1994) on negative viscosity, to the inclusion of nonlinear effects in the model, to possible extensions of our results, and to related work based on closure techniques.

2. Non-dimensional equations

We start with the linearized two-dimensional quasi-geostrophic equation, including free-surface and β effects, topography, Ekman friction and a viscous term that parameterizes turbulent dissipation. In dimensional form, this equation is written as

$$\partial_t \left(\nabla^2\psi - R^{-2}\psi\right) + \beta\partial_x\psi + \frac{f}{h}\boldsymbol{z}\cdot(\nabla\eta\times\nabla\psi) + r\nabla^2\psi - \nu\nabla^4\psi = 0, \tag{2.1}$$

where ψ is the streamfunction, $\boldsymbol{z}$ a unit vertical vector, r the Ekman friction coefficient and ν the eddy viscosity (see e.g. Pedlosky 1987, p. 233). The local Coriolis parameter and total ocean depth have been taken as $f+\beta y$ and $h+\eta$, where f, β and h are constants and $h \gg \eta$; the Rossby radius of deformation R is defined by $R := \sqrt{gh}/f$.

https://doi.org/10.1017/S0022112099007430 Published online by Cambridge University Press

In order to encompass various regimes with the same scaling, (2.1) is non-dimensionalized in a slightly unconventional way. We introduce a characteristic length L, whose interpretation varies with the regime (see below) and a parameter μ such that the spatial scale of the motion is given by $\mu^{-1}L$. The horizontal scale of the topography is then taken as $L_t = \epsilon\mu^{-1}L$, with $\epsilon \ll 1$. Using $\mu^{-1}L$, $\mu^{-2}f^{-1}$ and h as reference length, time and height, respectively, (2.1) is rewritten in dimensionless form by performing the substitutions

$$\left.\begin{aligned} &\boldsymbol{x} \to \mu^{-1}L\boldsymbol{x}, \quad t \to \mu^{-2}f^{-1}t, \quad \beta \to \mu f L^{-1}\beta, \\ &\eta \to h\eta, \quad r \to fr, \quad \nu \to \epsilon^2\mu^{-2}L^2 f\nu, \end{aligned}\right\} \tag{2.2}$$

leading to

$$\partial_t\left(\mu^2\nabla^2\psi - \lambda^2\psi\right) + \beta\partial_x\psi + \boldsymbol{z}\cdot(\nabla\eta\times\nabla\psi) + r\nabla^2\psi - \epsilon^2\nu\nabla^4\psi = 0, \tag{2.3}$$

where $\lambda := LR^{-1}$ and

$$\eta = \eta(\epsilon^{-1}\boldsymbol{x}). \tag{2.4}$$

Equation (2.3) may be employed to study the following regimes: (i) $\mu \ll 1$, $\lambda = O(1)$, corresponding to motion with a scale much larger than the radius of deformation; and (ii) $\mu \sim \lambda = O(1)$, corresponding to motion with a spatial scale of the order of the radius of deformation. In case (i), which we refer to as the long-wave regime, L has the order of magnitude of the radius of deformation, whereas in case (ii), which we refer to as the short-wave regime, L has the order of magnitude of the spatial scale of the motion. Note that the standard rigid lid approximation is obtained as a limiting case of (ii) with $\lambda \ll 1$.

The scaling factors proportional to μ in (2.2) have been chosen so that the β-effect, topography and Ekman friction all appear in (2.3) at leading order in μ. This choice ensures that the three effects have a similar importance in both the short-wave and the long-wave regimes – in that sense it is the most general. In order for the turbulent dissipation to affect only the small-scale motion (with scale L_t), the eddy viscosity ν has been rescaled by a factor ϵ^2. We emphasize that topography scale L_t is assumed small compared to the scale of the motion $\mu^{-1}L$, but not necessarily small compared to L; for the long-wave regime, in particular, the choice $\epsilon = \mu$ leads to a topography scale equal to L and of the order of the radius of deformation.

The essential feature of our scaling is that the potential-vorticity gradient associated with the topography is much larger ($O(\epsilon^{-1})$) than that associated with the β-effect. This is immediately apparent from (2.3) when one notes that $\nabla\eta = O(\epsilon^{-1})$. In terms of the dimensional variables, this indicates that

$$\beta \sim \epsilon\frac{f\eta}{hL_t},$$

or, using $\beta \sim f/a$, where a is the Earth's radius,

$$\frac{L_t h}{a\eta} \sim \epsilon \ll 1.$$

In the latter form, our scaling assumption can be interpreted as the requirement that the characteristic slope of the topography η/L_t is much larger than the aspect ratio of the ocean h/a – the topography is thus relatively steep. Under this assumption, which is satisfied in many areas of the world's oceans, the small-scale topography has a leading-order effect on the large-scale quasi-geostrophic motion. A significantly shallower topography as considered, for instance, by Thomson (1975) and Prahalad &

https://doi.org/10.1017/S0022112099007430 Published online by Cambridge University Press

Sengupta (1986), has a much weaker effect and affects the quasi-geostrophic motion over distances and times that are long compared to the typical spatial and temporal scales of the motion.

3. Multiple-scale analysis

Our objective in this section is to derive from (2.3) an approximate evolution equation for the large-scale quasi-geostrophic motion that implicitly accounts for the effect of the small-scale topography. To this end, we employ the standard multiple-scale technique (e.g. Hinch 1991), also known as homogenization in certain contexts (e.g. Bensoussan, Lions & Papanicolaou 1989). We slightly extend (2.4) and consider a topography that can have large-scale changes in addition to small-scale fluctuations, i.e. $\eta = \eta(\boldsymbol{x}, \epsilon^{-1}\boldsymbol{x})$. Introducing $\boldsymbol{X} := \epsilon^{-1}\boldsymbol{x}$ as the fast spatial variable, we decompose η into slowly and rapidly varying parts according to

$$\eta = \overline{\eta}(\boldsymbol{x}) + \eta'(\boldsymbol{x}, \boldsymbol{X}),$$

with $\overline{\eta} = \langle \eta \rangle$ and $\langle \eta' \rangle = 0$, where $\langle \cdot \rangle$ is a suitably defined average. Hereafter, we omit the prime and denote the small-scale component of the topography simply by η. We assume that this component is a periodic function of $\boldsymbol{X}$, in which case the average is the spatial average over the period.† It should be emphasized that the periodicity requirement applies to the small-scale topography only: the (large-scale) flow domain, and the large-scale topography can be arbitrary.

Introducing the transformation $\nabla \to \epsilon^{-1}\nabla_{\boldsymbol{X}} + \nabla$ into (2.3), we seek a solution in the form of a power series

$$\psi = \psi^{(0)}(\boldsymbol{x}, \boldsymbol{X}, t) + \epsilon\psi^{(1)}(\boldsymbol{x}, \boldsymbol{X}, t) + \epsilon^2\psi^{(2)}(\boldsymbol{x}, \boldsymbol{X}, t) + \cdots .$$

Substituting this expansion, one finds at order $O(\epsilon^{-2})$,

$$\mathscr{A}\psi^{(0)} = 0,$$

where

$$\mathscr{A} = \mu^2\partial_t\nabla_{\boldsymbol{X}}^2 + \boldsymbol{z} \cdot (\nabla_{\boldsymbol{X}}\eta \times \nabla_{\boldsymbol{X}}) + r\nabla_{\boldsymbol{X}}^2 - \nu\nabla_{\boldsymbol{X}}^4.$$

A solution is simply $\psi^{(0)} = \psi^{(0)}(\boldsymbol{x}, t)$, i.e. the leading-order streamfunction depends only on the slow spatial variables. At order $O(\epsilon^{-1})$ one finds

$$\mathscr{A}\psi^{(1)} = -\boldsymbol{z} \cdot \left(\nabla_{\boldsymbol{X}}\eta \times \nabla\psi^{(0)}\right). \tag{3.1}$$

In general, $\psi^{(1)}$ is given as a convolution: assuming $\psi^{(1)}(\boldsymbol{x}, \boldsymbol{X}, 0) = 0$, it has the form

$$\psi^{(1)}(\boldsymbol{x}, \boldsymbol{X}, t) = \int_0^t \boldsymbol{w}(\boldsymbol{x}, \boldsymbol{X}, t-\tau) \cdot \nabla\psi^{(0)}(\boldsymbol{x}, \tau)\,\mathrm{d}\tau + \overline{\psi^{(1)}}(\boldsymbol{x}, t), \tag{3.2}$$

where the average part $\overline{\psi^{(1)}}(\boldsymbol{x}, t)$ is so far undetermined. The kernel vector $\boldsymbol{w}(\boldsymbol{x}, \boldsymbol{X}, \tau)$ is the periodic, zero-mean solution of

$$\mathscr{A}\boldsymbol{w} = -(\boldsymbol{z} \times \nabla_{\boldsymbol{X}}\eta)\ \delta(\tau), \quad \text{with } \boldsymbol{w}(\boldsymbol{x}, \boldsymbol{X}, 0) = 0, \tag{3.3}$$

and is well defined in principle.

† The more sophisticated situation where η is almost-periodic can be treated with no essential modification; the random case is somewhat more delicate (cf. Papanicolaou 1995).

https://doi.org/10.1017/S0022112099007430 Published online by Cambridge University Press

Returning to the expansion of (2.3), we impose a solvability condition for $\psi^{(2)}$ by averaging the $O(1)$ equation. This leads to an evolution equation for $\psi^{(0)}$, namely

$$\partial_t(\mu^2\nabla^2\psi^{(0)} - \lambda^2\psi^{(0)}) + \beta\partial_x\psi^{(0)} + \boldsymbol{z}\cdot(\nabla\overline{\eta}\times\nabla\psi^{(0)}) + r\nabla^2\psi^{(0)} + \boldsymbol{z}\cdot\langle\nabla_{\boldsymbol{X}}\eta\times\nabla\psi^{(1)} + \nabla\eta\times\nabla_{\boldsymbol{X}}\psi^{(1)}\rangle = 0. \tag{3.4}$$

Using (3.2), this equation is rewritten as

$$\partial_t(\mu^2\nabla^2\psi^{(0)} - \lambda^2\psi^{(0)}) + \beta\partial_x\psi^{(0)} + \boldsymbol{z}\cdot(\nabla\overline{\eta}\times\nabla\psi^{(0)}) + r\nabla^2\psi^{(0)} + \nabla\cdot\int_0^t \boldsymbol{r}_{\mathrm{t}}(\boldsymbol{x}, t-\tau)\cdot\nabla\psi^{(0)}(\boldsymbol{x},\tau)\,\mathrm{d}\tau = 0, \tag{3.5}$$

where the tensor $\boldsymbol{r}_{\mathrm{t}}$ is given by

$$\boldsymbol{r}_{\mathrm{t}} = \langle(\boldsymbol{z}\times\nabla_{\boldsymbol{X}}\eta)\,\boldsymbol{w}\rangle \tag{3.6}$$

and $\boldsymbol{w}$ satisfies the auxiliary equation (3.3).

Equation (3.5), which governs the evolution of the large-scale, leading-order streamfunction, is the central result of this paper. Its first line contains all the terms of the original equation (2.3) except for the eddy viscosity term, but the topography that appears explicitly is the averaged topography $\overline{\eta}$. The effect of the small-scale topography, or more precisely of its interaction with the Ekman friction and turbulent dissipation, is described by the convolution term on the second line. As we discuss in detail below, this is an additional dissipative term which, in the short-wave regime, depends on the history of the large-scale flow; as a consequence $\psi^{(0)}$ obeys an integro-differential rather than differential equation. In the long-wave regime $\mu\to 0$, however, $\boldsymbol{r}_{\mathrm{t}}(\boldsymbol{x},\tau)\to\tilde{\boldsymbol{r}}(\boldsymbol{x})\delta(\tau)$ for a suitably defined $\tilde{\boldsymbol{r}}$, because (3.3) does not involve a time derivative; the additional term thus becomes a simple (possibly anisotropic and space-dependent) Ekman friction. We first consider this regime as it is very relevant physically and proves easily tractable.

4. Long-wave regime

In the long-wave limit $\mu\to 0$, the evolution equation (3.5) simplifies to

$$-\lambda^2\partial_t\psi^{(0)} + \beta\partial_x\psi^{(0)} + \boldsymbol{z}\cdot(\nabla\overline{\eta}\times\nabla\psi^{(0)}) + r\nabla^2\psi^{(0)} + \nabla\cdot(\tilde{\boldsymbol{r}}\cdot\nabla\psi^{(0)}) = 0. \tag{4.1}$$

The Ekman friction tensor $\tilde{\boldsymbol{r}}$, defined by $\boldsymbol{r}_{\mathrm{t}}(\boldsymbol{x},\tau) = \tilde{\boldsymbol{r}}(\boldsymbol{x})\delta(\tau)$ is given by

$$\tilde{\boldsymbol{r}} = \langle(\boldsymbol{z}\times\nabla_{\boldsymbol{X}}\eta)\,\tilde{\boldsymbol{w}}\rangle, \tag{4.2}$$

where $\tilde{\boldsymbol{w}}$ is such that $\boldsymbol{w}(\boldsymbol{x},\boldsymbol{X},\tau) = \tilde{\boldsymbol{w}}(\boldsymbol{x},\boldsymbol{X})\delta(\tau)$ and satisfies the auxiliary equation

$$(\mathscr{L} + r)\,\tilde{\boldsymbol{w}} = -\nabla_{\boldsymbol{X}}^{-2}(\boldsymbol{z}\times\nabla_{\boldsymbol{X}}\eta), \tag{4.3}$$

with

$$\mathscr{L} := \nabla_{\boldsymbol{X}}^{-2}[\boldsymbol{z}\cdot(\nabla_{\boldsymbol{X}}\eta\times\nabla_{\boldsymbol{X}})] - \nu\nabla_{\boldsymbol{X}}^2, \tag{4.4}$$

and $\langle\tilde{\boldsymbol{w}}\rangle = 0$. (Equation (4.3) is derived from (3.3) by applying the operator $\nabla_{\boldsymbol{X}}^{-2}$ which is well-defined when acting on zero-mean functions as is the case here; its form proves convenient in the next section when we compare the short- and long-wave regimes.)

When the small-scale topography $\eta(\boldsymbol{x},\boldsymbol{X})$ is given, the Ekman friction tensor $\tilde{\boldsymbol{r}}$ can be computed from (4.2) by first solving the linear differential equation (4.3) for a periodic $\tilde{\boldsymbol{w}}$. Because its coefficients depend on $\boldsymbol{X}$, this equation can only be solved

https://doi.org/10.1017/S0022112099007430 Published online by Cambridge University Press

numerically in general.† However, some properties of $\tilde{\boldsymbol{r}}$ may be derived directly from (4.2)–(4.3). We discuss them before presenting numerical results.

4.1. *Properties of* $\tilde{\boldsymbol{r}}$

We first remark that (4.3) becomes ill posed when $r = \nu = 0$. To see this, note that with $r = \nu = 0$ the general solution of (4.3) takes the closed form

$$\tilde{\boldsymbol{w}}(\boldsymbol{x}, \boldsymbol{X}) = -\boldsymbol{X} + \boldsymbol{\Phi}[\eta(\boldsymbol{x}, \boldsymbol{X})],$$

where $\boldsymbol{\Phi}[\cdot]$ is an arbitrary vector function. It is clear that it is not possible to choose $\boldsymbol{\Phi}$ so that $\tilde{\boldsymbol{w}}$ is a periodic, zero-mean function of $\boldsymbol{X}$. Equation (4.3) has thus no satisfactory solution when $r = \nu = 0$. This shows the importance of including dissipative effects, either Ekman friction or viscous dissipation, at leading order in the original equation (2.1).

Next we establish that $\tilde{\boldsymbol{r}}$ is positive definite. This is essential because it guarantees that the effect of the small-scale topography, parameterized by the last term in (4.1), is dissipative as could be expected on physical grounds. Consider the scalar $\boldsymbol{v} \cdot \tilde{\boldsymbol{r}} \cdot \boldsymbol{v}$, for an arbitrary vector $\boldsymbol{v}$ depending on $\boldsymbol{x}$ only. The following equalities follow from (4.2)–(4.3) using integration by parts:

$$\begin{aligned}\boldsymbol{v} \cdot \tilde{\boldsymbol{r}} \cdot \boldsymbol{v} &= -\langle \nabla_{\boldsymbol{X}}^2 [(\mathscr{L} + r)\boldsymbol{v} \cdot \tilde{\boldsymbol{w}}]\, \boldsymbol{v} \cdot \tilde{\boldsymbol{w}} \rangle \\ &= \langle -\partial(\eta, \boldsymbol{v} \cdot \tilde{\boldsymbol{w}})\, \boldsymbol{v} \cdot \tilde{\boldsymbol{w}} + r|\nabla_{\boldsymbol{X}}(\boldsymbol{v} \cdot \tilde{\boldsymbol{w}})|^2 + \nu|\nabla_{\boldsymbol{X}}^2(\boldsymbol{v} \cdot \tilde{\boldsymbol{w}})|^2 \rangle \\ &= \langle r|\nabla_{\boldsymbol{X}}(\boldsymbol{v} \cdot \tilde{\boldsymbol{w}})|^2 + \nu|\nabla_{\boldsymbol{X}}^2(\boldsymbol{v} \cdot \tilde{\boldsymbol{w}})|^2 \rangle > 0,\end{aligned}$$

where $\partial(\cdot, \cdot)$ is the Jacobian with respect to the fast variable $\boldsymbol{X}$. The positive definiteness of $\tilde{\boldsymbol{r}}$ then follows from the fact that both r and ν are positive.

In the spirit of Gama *et al.* (1994), we then study the restrictions on the form of $\tilde{\boldsymbol{r}}$ imposed by possible discrete symmetries of η. Consider transformations of the coordinates and of the topography of the form

$$\boldsymbol{X} \mapsto \boldsymbol{X}' = \boldsymbol{A}\boldsymbol{X}, \qquad \eta(\boldsymbol{x}, \boldsymbol{X}) \mapsto \pm\eta(\boldsymbol{x}, \boldsymbol{X}'),$$

where $\boldsymbol{A}$ is a constant tensor. If $\boldsymbol{A}$ is orthogonal, the Laplacian $\nabla_{\boldsymbol{X}}^2$ and thus the dissipative terms of (2.1) are invariant under the transformation; if in addition the topographic term $\boldsymbol{z} \cdot (\nabla_{\boldsymbol{X}}\eta \times \nabla_{\boldsymbol{X}}\psi)$ is invariant, then Ekman friction tensor $\tilde{\boldsymbol{r}}(\boldsymbol{x})$ is also invariant. It follows from the formula for the transformation of tensors that

$$\tilde{\boldsymbol{r}}(\boldsymbol{x}) = \boldsymbol{A}^{\mathrm{T}}\tilde{\boldsymbol{r}}(\boldsymbol{x})\boldsymbol{A}. \tag{4.5}$$

Constraints on the coefficients of $\tilde{\boldsymbol{r}}$ are readily derived from this expression. Table 1 gives the form of $\tilde{\boldsymbol{r}}$ obtained for some particular symmetries. Note that the origin of the coordinate system (X, Y) can be chosen arbitrarily – useful choices ensure that the origin is a centre of symmetry for η. Note also that when η does not depend on the large-scale coordinates $\boldsymbol{x}$, $\tilde{\boldsymbol{r}}$ can be symmetrized. When in addition $\eta(X, Y) = \eta(Y, -X)$, $\tilde{\boldsymbol{r}}$ becomes proportional to the identity tensor, indicating that the effect of the small-scale topography is simply to renormalize the original Ekman friction coefficient r.

Two final observations can be made about the scaling of $\tilde{\boldsymbol{r}}$. First, it is obvious from (4.2)–(4.3) that $\tilde{\boldsymbol{r}}$ depends on the amplitude of the topography in a non-trivial

† Analytical expressions for $\tilde{\boldsymbol{r}}$ and more generally for $\boldsymbol{r}_{\mathrm{t}}(\tau)$ can be derived for topographies consisting of isolated features with simple, step-like profiles when the distance between these features is asymptotically large. This is used in Vanneste (2000) for an explicit calculation of the change in Rossby-wave frequency that is induced by topography in the short-wave regime.

https://doi.org/10.1017/S0022112099007430 Published online by Cambridge University Press

Symmetry	$\tilde{\boldsymbol{r}}$
$\eta(X,Y) = -\eta(Y,X)$	$\begin{pmatrix} a & b \\ b & a \end{pmatrix}$
$\eta(X,Y) = \eta(Y,-X)$	$\begin{pmatrix} a & b \\ -b & a \end{pmatrix}$
$\eta(X,Y) = -\eta(-X,Y)$	$\begin{pmatrix} a & 0 \\ 0 & b \end{pmatrix}$

TABLE 1. Form of the Ekman friction tensor $\tilde{\boldsymbol{r}}$ when the topography $\eta(\boldsymbol{x},\boldsymbol{X})$ is invariant under particular transformations of the fast spatial coordinates $\boldsymbol{X}$. a and b are real functions of $\boldsymbol{x}$.

way. However, it can be verified that under the transformation $(\eta, r, \nu) \mapsto \alpha(\eta, r, \nu)$, where α is a constant, the topography-induced Ekman friction tensor transforms according to $\tilde{\boldsymbol{r}} \mapsto \alpha\tilde{\boldsymbol{r}}$. It is therefore sufficient to consider the dependence of $\tilde{\boldsymbol{r}}$ on r and ν for a fixed amplitude of the topography. Second, (4.2)–(4.3) indicates that $\tilde{\boldsymbol{r}}$ is independent of the scale of the topography if the viscosity vanishes. More specifically, it can be shown that the transformation $\eta(\boldsymbol{x},\boldsymbol{X}) \mapsto \eta(\boldsymbol{x},\alpha\boldsymbol{X}), \nu \mapsto \alpha^{-2}\nu$, leaves $\tilde{\boldsymbol{r}}$ unchanged. Since we expect the influence of the Ekman friction to dominate over that of the turbulent dissipation away from horizontal boundaries, this suggests that the topography-induced dissipation in the ocean's interior may depend only weakly on the scale of the topography.

4.2. *Numerical computation of* $\tilde{\boldsymbol{r}}$

We illustrate the theoretical results of the previous section by computing $\tilde{\boldsymbol{r}}$ for specific choices of the topography. For simplicity we consider topographies that are independent of the large-scale coordinates $\boldsymbol{x}$. The results can nevertheless be employed if the amplitude of the topography (but not its shape) is changing on the large scale by taking advantage of the scaling transformation $(\eta, r, \nu) \mapsto \alpha(\eta, r, \nu)$ described in § 4.1.

Equation (4.3) is solved numerically by expanding η and $\tilde{\boldsymbol{w}}$ in truncated Fourier series. Both functions have a vanishing mean, so that their expansions do not include the wavevector $(0,0)$. Introducing the Fourier expansions in (4.3) and projecting on each mode leads to a linear system of equations for the Fourier components of $\tilde{\boldsymbol{w}}$. Once this system is solved, $\tilde{\boldsymbol{r}}$ is easily computed from (4.2). When the expansion of η contains only a few modes, the matrix associated with this linear system is sparse and efficient numerical techniques can be employed to compute the solution. The number of Fourier modes retained in the expansion of $\tilde{\boldsymbol{w}}$ depends on the form of η and is chosen large enough for its influence on the results to be insignificant. Typically we have used 40 wavenumbers in each direction, corresponding to $4 \times 40 \times 40 = 6400$ real coefficients in the expansion of $\tilde{\boldsymbol{w}}$.

The first topography we consider is

$$\eta = \cos X \cos Y. \tag{4.6}$$

The symmetries of this topography together with table 1 indicate that $\tilde{\boldsymbol{r}}$ is proportional to the identity tensor, i.e. $\tilde{\boldsymbol{r}} = \tilde{r}\boldsymbol{I}$. The scalar $\tilde{r}$ completely characterizes the enhancement of dissipation due to topography. Figure 1 shows the dependence of $\tilde{r}$ on the original Ekman friction coefficient r for different values of the eddy viscosity ν. Note that the maximum value of $\tilde{r}$ is attained either at $r = 0$ or at intermediate r, depending on ν,

https://doi.org/10.1017/S0022112099007430 Published online by Cambridge University Press

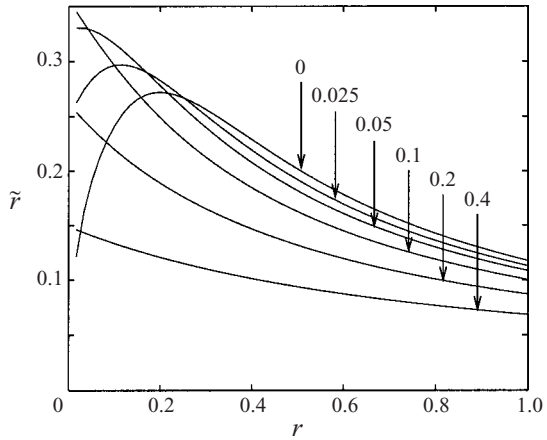


FIGURE 1. Topography-induced Ekman friction coefficient $\tilde{r}$ as a function of the original Ekman friction coefficient r for the topography $\eta = \cos X \cos Y$. The different curves correspond to the different values of the viscosity ν indicated by the arrows.

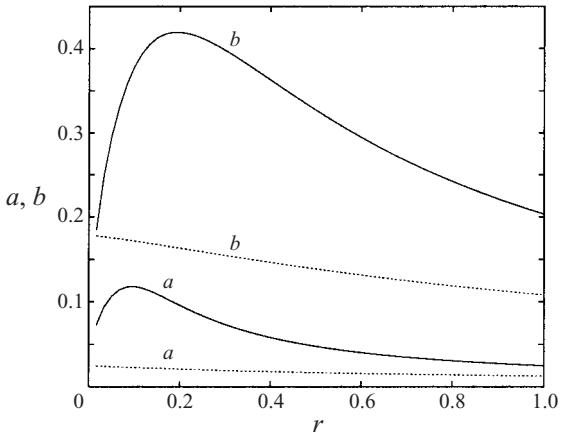


FIGURE 2. Components of the topography-induced Ekman friction tensor $\tilde{\boldsymbol{r}} = \mathrm{diag}\,(a, b)$ as a function of the Ekman friction coefficient r for the topography $\eta = \sin(3X)\sin Y$. Results obtained with viscosity $\nu = 0$ (solid curves) and $\nu = 0.025$ (dotted curves) are displayed.

while $\tilde{r}$ systematically decreases for large r. In general $\tilde{r}$ tends to a finite value when $r \to 0$; it is not so, however, when $\nu = 0$, in which case $\tilde{r} \to 0$ as $r \to 0$ (see next section).

Although in practice the value of $\tilde{r}$ depends on the maximum amplitude of the topography, taken here equal to unity, it is clear from figure 1 that the topography-induced Ekman friction may be of the same order as or larger than the original Ekman friction and may thus have a significant impact on the large-scale quasi-geostrophic motion.

As a second illustration we consider the anisotropic topography

$$\eta = \sin(3X)\sin Y. \tag{4.7}$$

According to table 1, the corresponding Ekman friction tensor is diagonal: $\tilde{\boldsymbol{r}} = \mathrm{diag}\,(a, b)$. Figure 2 shows the two coefficients a and b as a function of r for $\nu = 0$ and

https://doi.org/10.1017/S0022112099007430 Published online by Cambridge University Press

$\nu = 0.025$. The two coefficients have very different magnitudes: a, which is associated with the direction of the smaller scale of the topography, is significantly smaller than b, which is associated with the direction of the larger scale. Comparison with the results obtained with the isotropic topography (4.6) suggests that the (turbulent) viscous dissipation has a stronger impact when the topography is anisotropic. To make such a comparison meaningful, we should use isotropic and anisotropic topographies with similar total wavenumbers; this is not the case of (4.6) and (4.7) which have total wavenumbers $\sqrt{2}$ and $\sqrt{10}$, respectively. However, we can exploit the transformation property discussed in § 4.1 and infer that the value of $\tilde{r}$ for the isotropic topography $\eta = \cos(\sqrt{5}X)\cos(\sqrt{5}Y)$ (which has the same total wavenumber $\sqrt{10}$ as (4.7)) for $\nu = 0.025$ is the same as that obtained for (4.6) with $\nu = 5 \times 0.025 = 0.125$. Figure 1 shows $\tilde{r}$ for the close value $\nu = 0.1$; comparison with the curves on figure 2 corresponding to $\nu = 0.025$ reveals the stronger influence of viscous dissipation in the anisotropic case, leading to small values for a and b and to their weak dependence on r.

The two examples above emphasize the subtle relationship that exists between the strength of the dissipation mechanisms originally present in the system (Ekman friction and turbulent dissipation) and the importance of their enhancement by topography. To gain insight into this relationship we now study the dependence of $\tilde{\boldsymbol{r}}$ on r and ν when these parameters are asymptotically large or small.

4.3. *Asymptotic form of* $\tilde{\boldsymbol{r}}$

When r, ν or both are large, $\tilde{\boldsymbol{r}}$ can be computed using a regular perturbation expansion. Although such an expansion can easily be carried out to higher order (for instance to provide an analytic expression for $\tilde{\boldsymbol{r}}$ valid for r or ν only moderately large, cf. Gama *et al.* 1994), we derive the leading-order term only. Let $\Gamma \gg 1$ be a large parameter and assume that $r \sim \nu = O(\Gamma)$. The solution to (4.3) can be sought as an expansion in inverse powers of Γ, namely

$$\tilde{\boldsymbol{w}} = \Gamma^{-1}\tilde{\boldsymbol{w}}_1 + \Gamma^{-2}\tilde{\boldsymbol{w}}_2 + \cdots .$$

The leading-order solution is clearly

$$\tilde{\boldsymbol{w}}_1 = -\boldsymbol{z} \times \left[\left(\frac{r}{\Gamma} - \frac{\nu}{\Gamma}\nabla_X^2\right)^{-1} \nabla_X^{-2}\eta\right],$$

leading to the approximation

$$\tilde{\boldsymbol{r}} = -\left\langle (\boldsymbol{z} \times \nabla_X \eta)\, \boldsymbol{z} \times \left[\left(r - \nu\nabla_X^2\right)^{-1} \nabla_X^{-2}\eta\right]\right\rangle + O(\Gamma^{-2}) \tag{4.8}$$

for the Ekman friction tensor. Clearly, $\tilde{\boldsymbol{r}}$ is inversely proportional to r and ν. The form of $\tilde{\boldsymbol{r}}$ is particularly simple when η is an eigenfunction of the Laplacian, i.e. when

$$\nabla_X^2\eta = -\Lambda^2\eta$$

for some Λ, as is the case for (4.6) and (4.7). It is indeed easy to show that (4.8) becomes

$$\tilde{\boldsymbol{r}} = \frac{1}{\Lambda^2(r + \nu\Lambda^2)}\langle(\boldsymbol{z} \times \nabla_X\eta)(\boldsymbol{z} \times \nabla_X\eta)\rangle.$$

Figure 3 confirms this asymptotic approximation through a comparison with numerical results for the topography (4.6) for which $\tilde{\boldsymbol{r}} = \tilde{r}\boldsymbol{I}$. We note that the asymptotic solution converges rapidly to the numerical one as r increases, and that moderate

https://doi.org/10.1017/S0022112099007430 Published online by Cambridge University Press

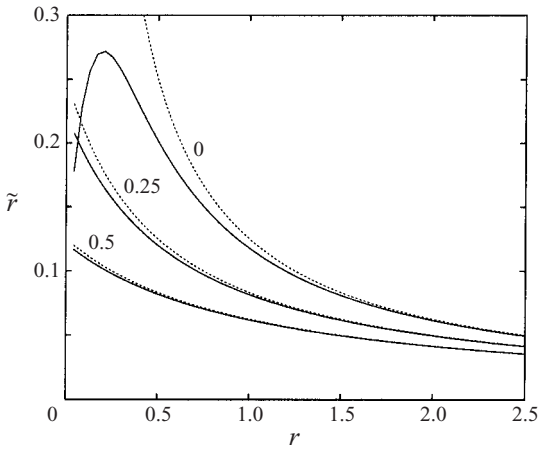


FIGURE 3. Topography-induced Ekman friction coefficient $\tilde{r}$ as a function of the Ekman friction coefficient r for the topography $\eta = \cos X \cos Y$, with $\nu = 0, 0.25$ and 0.5. The numerical solution (solid curves) is compared to the asymptotic solution (dotted curves) valid for large r or ν.

values of ν are sufficient for the asymptotic solution to be a good approximation even at small r.

In the opposite limit of small r and ν, the derivation of the asymptotic form of $\tilde{\boldsymbol{r}}$ necessitates the use of a singular-perturbation technique. This is because (4.3) with $r = \nu = 0$ is ill posed, as demonstrated in §4.1. The asymptotics may depend on the details of the topography; for definiteness and simplicity we consider the topography (4.6). We first treat the case $\nu \ll r \ll 1$ for which the viscous dissipation can be ignored. The two components of (4.3) may then be regarded as forced advection–diffusion equations, interpreting η as the flow streamfunction, the components of $\tilde{\boldsymbol{w}}$ as scalar concentrations, and r as the diffusivity. With this interpretation, our problem becomes analogous to the determination of an effective diffusivity for the transport of passive scalars in time-independent, space-periodic flows in the small-diffusivity (large-Péclet-number) limit. The latter problem has been studied in detail by Rosenbluth *et al.* (1987) and Shraiman (1987). These authors concluded from a boundary-layer analysis that the effective diffusivity scales like the square root of the diffusivity. Here, we can similarly conclude that

$$\tilde{\boldsymbol{r}} \sim r^{1/2}. \tag{4.9}$$

As indicated by the work of Rosenbluth *et al.* (1987) and Shraiman (1987), the explicit derivation of the proportionality constants would be tedious and yield final results that need to be evaluated numerically in general. Therefore we do not attempt this derivation; we nevertheless explain the origin of the scaling (4.9) and confirm its validity numerically.

The topography (4.6) consists of a periodic juxtaposition of hills and hollows bounded by separatrices on which $\eta = 0$. A piecewise solution to (4.3) with $r = \nu = 0$ is given by

$$\tilde{\boldsymbol{w}} = -\boldsymbol{X} + \boldsymbol{\Phi}_i, \tag{4.10}$$

where $\boldsymbol{\Phi}_i$ are constant vectors in each hill or hollow which we label by i. These vectors can be chosen to ensure that the average of $\tilde{\boldsymbol{w}}$ vanishes. A valid solution to (4.3), however, needs to be smooth everywhere, and hence must differ from (4.10) near the separatrices. In the vicinity of the separatrices a boundary layer forms in which the

https://doi.org/10.1017/S0022112099007430 Published online by Cambridge University Press

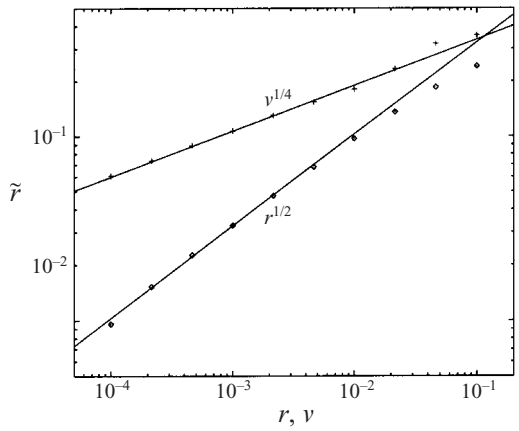


FIGURE 4. Topography-induced Ekman friction coefficient $\tilde{r}$ as a function of r for $v = 0$ (diamonds) and as a function of v for $r = 0$ (crosses) for the topography $\eta = \cos X \cos Y$. The straight lines indicates the power laws $r^{1/2}$ and $v^{1/4}$ valid in the asymptotic regimes $v \ll r \ll 1$ and $r \ll v \ll 1$, respectively.

Ekman friction is not negligible so as to allow the smooth transition between each hill or hollow. The boundary-layer width scales like $r^{-1/2}$. This is seen by writing (4.3) near the separatrices using η and an angle-like variable θ as independent coordinates, following Rosenbluth *et al.* (1987). Neglecting derivatives along topography lines in the Laplacian leads to

$$\frac{\partial \tilde{\boldsymbol{w}}}{\partial \theta} + r \frac{\partial}{\partial \eta} \left(\frac{|\nabla_X \theta|}{|\nabla_X \eta|} \frac{\partial \tilde{\boldsymbol{w}}}{\partial \eta} \right) = -\boldsymbol{z} \times \nabla_X \eta.$$

It is clear from this equation that the Ekman-friction term with $r \ll 1$ can balance the other terms provided that changes of order unity in $\tilde{\boldsymbol{w}}$ take place over spatial scales of order $r^{1/2}$ in the direction of η, i.e. provided that a boundary layer of width $r^{1/2}$ forms. Now, in the calculation of $\tilde{\boldsymbol{r}} = \tilde{r}\boldsymbol{I}$ from (4.2) it can be verified using integration by parts and the vanishing of η on separatrices that the contribution of (4.10) (which neglects the boundary layers) vanishes. At leading order $\tilde{r}$ is therefore determined by the contribution of the boundary layers, and it is thus proportional to their width, $r^{1/2}$.

To verify the validity of this argument, we have computed $\tilde{r}$ numerically for small values of r with $v = 0$. The result, displayed in figure 4, confirms the power-law scaling $\tilde{r} \sim r^{1/2}$. (Note that a high resolution is required for accurate results with weak dissipation; a truncation using 120×120 Fourier modes has been employed for the calculation corresponding to the two smallest values of r.)

In the regime $r \ll v \ll 1$ where the Ekman friction is negligible, a boundary-layer approach similar to that sketched above can also be employed, providing the power-law scaling $\tilde{r} \sim v^{1/4}$. This scaling has also been confirmed by numerical computations with $r = 0$ and the results are displayed in figure 4. We emphasize that the power-law results are valid only for topographies of the type (4.6) with closed contour lines and $\eta = 0$ at separatrices. For different topographies, in particular with open contour lines, $\tilde{\boldsymbol{r}}$ can tend to a constant as r or v tend to zero. In any case our results indicate that the topography-induced Ekman friction dominates over the original friction mechanisms when these become vanishingly weak.

https://doi.org/10.1017/S0022112099007430 Published online by Cambridge University Press

5. Short-wave regime

We now return to the evolution equation for the large-scale streamfunction (3.5) valid in the short-wave regime $\mu = O(1)$. In this regime, the effect induced by the topography is clearly more complex than a simple additional Ekman friction, since it is described by a convolution term that depends on the history of the large-scale flow. In this section we study some of the properties of this convolution term.

It is interesting to note that linear integro-differential equations similar to (3.5) appear in other areas of physics, notably in the theory of heat conduction with finite propagation speed (e.g. Gurtin & Pipkin 1968). The work of Miller (1978) establishing the existence, uniqueness and continuity of solutions provides a particularly useful reference for our problem.

The behaviour of (3.5) depends on the kernel $\boldsymbol{r}_{\mathrm{t}}(\boldsymbol{x},\tau)$. To obtain this kernel from (3.6), equation (3.3) governing the time evolution of $\boldsymbol{w}$ needs to be solved first. Although this ultimately requires numerical calculation, some progress can be made by using the Laplace transform. Denoting Laplace transforms by a caret and the Laplace variable by u, we transform (3.3) and (3.6) into

$$(\mathscr{L}+\mu^2 u+r)\hat{\boldsymbol{w}} = -\nabla_X^{-2}(\boldsymbol{z}\times\nabla_X\eta), \tag{5.1}$$

and

$$\hat{\boldsymbol{r}}_{\mathrm{t}} = \langle(\boldsymbol{z}\times\nabla_X\eta)\,\hat{\boldsymbol{w}}\rangle, \tag{5.2}$$

with $\mathscr{L}$ defined by (4.4). Comparing (5.1) with (4.3) indicates that $\hat{\boldsymbol{w}}$ satisfies the same equation as the vector $\tilde{\boldsymbol{w}}$ employed in the long-wave regime but with $\mu^2 u+r$ replacing r; a similar relationship exists between $\hat{\boldsymbol{r}}_{\mathrm{t}}$ and $\tilde{\boldsymbol{r}}$. This implies that properties of $\tilde{\boldsymbol{r}}$, in particular the symmetry properties discussed in § 4.1, carry over to $\boldsymbol{r}_{\mathrm{t}}$. Of course, an essential difference is that $\tilde{\boldsymbol{w}}$ needs to be calculated for a fixed value of r, whereas $\hat{\boldsymbol{w}}$ needs to be calculated for $\mu^2 u+r$ on curves in the complex plane as is required for the Laplace inversion. More precisely, it is the analytic continuation of $\hat{\boldsymbol{w}}$ that is required, since (5.1) defines $\hat{\boldsymbol{w}}$ for $\mathrm{Re}\,(u) > -r$ only. The numerical computation of the analytic continuation of $\hat{\boldsymbol{w}}$ from (3.3) for u in the complex plane and its use for the Laplace inversion providing $\boldsymbol{r}_{\mathrm{t}}(\boldsymbol{x},\tau)$ represent a challenging problem whose treatment is beyond the scope of this paper. Here we only consider properties of $\boldsymbol{r}_{\mathrm{t}}$ that can be derived analytically.

5.1. *History dependence*

We first study the dependence of the dissipation-induced term on the flow history. This can be done by studying the decay of $\boldsymbol{r}_{\mathrm{t}}(\tau)$ as $\tau\to\infty$, since this decay characterizes the speed at which the memory of the flow history is lost. The Laplace inversion formula indicates that the time evolution of $\boldsymbol{r}_{\mathrm{t}}$ is governed by the singularities of $\hat{\boldsymbol{w}}$ in the complex u-plane. These are associated with the spectrum of $\mathscr{L}$; precisely, they are located where u is such that $-\mu^2 u-r$ belongs to the spectrum of $\mathscr{L}$. It can be shown using theorem IV-1.16 of Kato (1966) that $\mathscr{L}^{-1}$ is compact, and hence (see Kato 1966, theorem III-6.29) that the spectrum of $\mathscr{L}$ consists of a countable number of eigenvalues, l_n say ($n=1,2,\ldots$). Therefore the only singularities of $\hat{\boldsymbol{w}}(u)$ are poles at

$$u_n = -\frac{l_n+r}{\mu^2}, \quad n=1,2,\ldots, \tag{5.3}$$

https://doi.org/10.1017/S0022112099007430 Published online by Cambridge University Press

and the evolution of $\boldsymbol{r}_t(\tau)$ is typically exponential: assuming that all the eigenvalues are simple, $\boldsymbol{r}_t(\boldsymbol{x},\tau)$ takes the form

$$\boldsymbol{r}_t(\boldsymbol{x},\tau)=\sum_n \boldsymbol{C}_n(\boldsymbol{x})\exp(u_n\tau),$$

for some vector functions $\boldsymbol{C}_n(\boldsymbol{x})$.

An upper bound on the real part of the u_n can be derived. Consider the eigenvalue equation

$$(\mathscr{L}-l_n)v_n=0$$

for $\mathscr{L}$. Multiplying by $\nabla_{\boldsymbol{X}}^2 v_n^*$, applying the averaging operator $\langle\cdot\rangle$, and taking the real part gives

$$\mathrm{Re}(l_n)=\nu\frac{\langle|\nabla_{\boldsymbol{X}}^2 v_n|^2\rangle}{\langle|\nabla_{\boldsymbol{X}} v_n|^2\rangle}\geqslant \nu\Lambda_0^2,$$

where $-\Lambda_0^2$ is the largest eigenvalue of the Laplacian (acting on periodic zero-mean functions). From (5.3) we then derive the upper bound

$$\mathrm{Re}(u_n)\leqslant -\frac{r+\nu\Lambda_0^2}{\mu^2}<0,$$

which provides the time scale for the loss of memory in the system. Clearly, the memory is lost rapidly if r or ν are large, or if μ is small. As discussed in § 4, there is no memory when $\mu\to 0$ and the evolution is governed by a differential equation.

5.2. *Dissipative character*

It is important to confirm that the convolution term associated with the small-scale topography in (3.5) is dissipative and thus corresponds to an enhancement of the dissipation as anticipated. In the long-wave regime $\mu\to 0$, when the topography-induced term has the form of a standard Ekman friction, we established this by proving that $\tilde{\boldsymbol{r}}$ is positive definite, which implies a monotonic decrease of the energy of the flow. Here, in order to deal with the convolution, we take a sightly different approach and show directly that the topography-induced term causes an exponential damping of the streamfunction.

Consider the evolution of the potential vorticity associated with the convolution term only; it is governed by the equation

$$\partial_t(\mu^2\nabla^2\psi^{(0)}-\lambda^2\psi^{(0)})+\nabla\cdot\int_0^t \boldsymbol{r}_t(\boldsymbol{x},t-\tau)\cdot\nabla\psi^{(0)}(\boldsymbol{x},\tau)\,\mathrm{d}\tau=0$$

obtained from (3.5) by removing the terms associated with the β-effect, large-scale topography and dissipation. Using the Laplace transform, it is easy to show that the time dependence of $\psi^{(0)}$ takes the form $\hat{\psi}(\boldsymbol{x})\exp(ut)$, where u is an eigenvalue of the (generalized) eigenvalue problem

$$u(\mu^2\nabla^2\hat{\psi}-\lambda^2\hat{\psi})+\nabla\cdot(\hat{\boldsymbol{r}}_t\cdot\nabla\hat{\psi})=0. \tag{5.4}$$

We now establish that all solutions are such that $\mathrm{Re}(u)<0$, corresponding to the damping of ψ expected for a dissipative system. Multiplying the previous equation by $\hat{\psi}^*$, integrating over the (large-scale) fluid domain, and using the boundary conditions we find

$$u\int(\mu^2|\nabla\hat{\psi}|^2+\lambda^2|\hat{\psi}|^2)\,\mathrm{d}\boldsymbol{x}+\int\nabla\hat{\psi}^*\cdot\hat{\boldsymbol{r}}_t\cdot\nabla\hat{\psi}\,\mathrm{d}\boldsymbol{x}=0. \tag{5.5}$$

https://doi.org/10.1017/S0022112099007430 Published online by Cambridge University Press

Now (5.1)–(5.2) implies that for any complex vector $\boldsymbol{v}$ depending on $\boldsymbol{x}$ only,

$$\begin{aligned}\boldsymbol{v}^* \cdot \hat{\boldsymbol{r}}_\mathrm{t} \cdot \boldsymbol{v} &= -\boldsymbol{v}^* \cdot \langle \nabla_{\boldsymbol{X}}^2 (\mathscr{L} + \mu^2 u^* + r) \hat{\boldsymbol{w}}^* \hat{\boldsymbol{w}} \rangle \cdot \boldsymbol{v} \\ &= \langle -\partial(\eta, \boldsymbol{v}^* \cdot \hat{\boldsymbol{w}}^*) \boldsymbol{v} \cdot \hat{\boldsymbol{w}} + \left(\mu^2 u^* + r\right) |\nabla_{\boldsymbol{X}} (\boldsymbol{v} \cdot \hat{\boldsymbol{w}})|^2 + \nu |\nabla_{\boldsymbol{X}}^2 (\boldsymbol{v} \cdot \hat{\boldsymbol{w}})|^2 \rangle.\end{aligned}$$

On taking the real part it follows that

$$\mathrm{Re}\,\left(\boldsymbol{v}^* \cdot \hat{\boldsymbol{r}}_\mathrm{t} \cdot \boldsymbol{v}\right) = \langle (\mu^2 \mathrm{Re}\,(u) + r) |\nabla_{\boldsymbol{X}} (\boldsymbol{v} \cdot \hat{\boldsymbol{w}})|^2 + \nu |\nabla_{\boldsymbol{X}}^2 (\boldsymbol{v} \cdot \hat{\boldsymbol{w}})|^2 \rangle.$$

Letting $\boldsymbol{v} = \nabla \hat{\psi}$ in this expression and introducing it into the real part of (5.5) leads to an equation of the form

$$\mathrm{Re}\,(u) P = -Q,$$

where P and Q are both positive. We thus conclude that the eigenvalues u of (5.4) satisfy $\mathrm{Re}\,(u) < 0$ as claimed.

5.3. *Rossby waves for* $\mu \ll 1$

In this subsection, we consider (3.5) for $\mu \ll 1$ and investigate the effect of the topography-induced dissipation on Rossby-wave propagation using a perturbation expansion. Since $\mu = 0$ corresponds to the long-wave regime studied in § 3 for which the friction does not depend on the flow history, the history dependence appears only at $O(\mu^2)$ and affects slightly the wave propagation.

Starting with (3.5) (with $\overline{\eta} = 0$), we introduce a solution in the form of a wave:

$$\psi^{(0)} = \hat{\psi} \exp\left[\mathrm{i}(\boldsymbol{k} \cdot \boldsymbol{x} - \omega t)\right],$$

where $\boldsymbol{k} = (k_x, k_y)$ is a wavevector and ω a frequency. Assuming a small-scale topography that does not vary on the large scale and that is sufficiently symmetric so that $\boldsymbol{r}_\mathrm{t} = r_\mathrm{t} \boldsymbol{I}$, we obtain the dispersion relation

$$\omega(\mu^2 k^2 + \lambda^2) + k_x \beta + \mathrm{i} k^2 \left[r + \hat{r}_\mathrm{t}(-\mathrm{i}\omega)\right] = 0, \tag{5.6}$$

where $k = |\boldsymbol{k}|$ and $\hat{r}_\mathrm{t}(-\mathrm{i}\omega)$ is the Laplace transform of r_t (with $\hat{\boldsymbol{r}}_\mathrm{t} = \hat{r}_\mathrm{t} \boldsymbol{I}$) evaluated at $u = -\mathrm{i}\omega$. So far the hypothesis $\mu \ll 1$ has not been employed and (5.6) is the exact dispersion relation. It relates ω to $\boldsymbol{k}$ implicitly and may be solved numerically if $\hat{r}_\mathrm{t}(u)$ is known for u in the complex plane. Taking advantage of the hypothesis $\mu \ll 1$, however, we can solve (5.6) analytically by expanding ω and $\hat{r}_\mathrm{t}$ in powers of μ^2 according to

$$\omega = \omega_0 + \mu^2 \omega_1 + \cdots \quad \text{and} \quad \hat{r}_\mathrm{t}(u) = \tilde{r}_0 + \mu^2 u \tilde{r}_1 + \cdots .$$

In the above, the $\tilde{r}_n$, $n = 1, 2, \cdots$, do not depend on u: the dependence on u which emerges from (5.1)–(5.2) appears explicitly in the powers of $\mu^2 u$ multiplying the $\tilde{r}_n$. This also implies that the $\tilde{r}_n$ are real. Introducing these expansions into (5.6) leads to

$$\omega_0 = -\frac{\beta k_x}{\lambda^2} - \mathrm{i}\frac{k^2 (r + \tilde{r}_0)}{\lambda^2}, \qquad \omega_1 = -\frac{k^2}{\lambda^2} \omega_0 (1 + \tilde{r}_1), \cdots.$$

The leading-order frequency is the one found for long Rossby waves when an Ekman friction with coefficient $r + \tilde{r}_0$ is taken into account. The coefficient $\tilde{r}_0$ describing the enhancement of the friction due to the small-scale topography is the same as $\tilde{r}$ computed in § 3. The correction ω_1 to the frequency consists of two terms. The first one (term 1 in the brackets) is usual: it is associated with the finite scale of the waves and is seen to emerge from the expansion in powers of μ^2 of the exact formula for the frequency $\omega = \lambda^2 \omega_0 / (\lambda^2 + \mu^2 k^2)$ that holds in the absence of dissipation. The second correction (term $\tilde{r}_1$ in the brackets) appears as a result of the history dependence.

https://doi.org/10.1017/S0022112099007430 Published online by Cambridge University Press

Using the assumed symmetry property, we can compute the $\tilde{r}_n$ from (5.1)–(5.2) using a single component of $\hat{\boldsymbol{w}}$, say the first one which we denote by $\hat{w}$. Expanding this component in powers of $\mu^2 u$ according to

$$\hat{w} = \tilde{w}_0 + \mu^2 u \tilde{w}_1 + \cdots$$

leads after introduction into (5.1) to the sequence of differential equations

$$\partial(\eta, \tilde{w}_0) + r\nabla_{\boldsymbol{X}}^2 \tilde{w}_0 - \nu\nabla_{\boldsymbol{X}}^4 \tilde{w}_0 = \partial_Y \eta,$$
$$\partial(\eta, \tilde{w}_1) + r\nabla_{\boldsymbol{X}}^2 \tilde{w}_1 - \nu\nabla_{\boldsymbol{X}}^4 \tilde{w}_1 = -\nabla_{\boldsymbol{X}}^2 \tilde{w}_0, \cdots$$

which need to be solved numerically. Once this is done, the $\tilde{r}_n$ are computed from

$$\tilde{r}_0 = -\langle \partial_Y \eta\, \tilde{w}_0 \rangle, \qquad \tilde{r}_1 = -\langle \partial_Y \eta\, \tilde{w}_1 \rangle, \cdots .$$

It does not appear that $\tilde{r}_1$ has a definite sign, so the qualitative effect of the history dependence may depend on the particular topography considered; in particular, the history dependence leads to a frequency shift of the waves which may have any sign. It is however possible to derive bounds on $\tilde{r}_1$ by simple manipulation of the equations above. Assuming $\nu = 0$ for simplicity, it is easy to establish the following equalities using integration by parts:

$$\tilde{r}_0 = r\langle |\nabla_{\boldsymbol{X}} w_0|^2 \rangle, \quad \tilde{r}_1 = \langle |\nabla_{\boldsymbol{X}} w_0|^2 + 2r\nabla_{\boldsymbol{X}} w_0 \cdot \nabla_{\boldsymbol{X}} w_1 \rangle,$$
$$\text{and} \quad r\langle |\nabla_{\boldsymbol{X}} w_1|^2 \rangle = -\langle \nabla_{\boldsymbol{X}} w_0 \cdot \nabla_{\boldsymbol{X}} w_1 \rangle.$$

The Cauchy–Schwartz inequality applied to the last equation gives $r^2\langle |\nabla_{\boldsymbol{X}} w_1|^2 \rangle \leqslant \langle |\nabla_{\boldsymbol{X}} w_0|^2 \rangle$. Further manipulations involving the other two equalities finally yield the useful bounds

$$-\frac{\tilde{r}_0}{r} \leqslant \tilde{r}_1 \leqslant \frac{\tilde{r}_0}{r}.$$

6. Concluding remarks

Our analysis is closely related to the various studies of negative viscosity in two-dimensional flows, in particular that of Gama *et al.* (1994), which are concerned with the evolution of large-scale flows superposed on small-scale currents. Both currents and topography are associated with a small-scale potential-vorticity gradient, but in addition currents introduce a small-scale advection. It turns out that the effects of the potential-vorticity gradient and advection on the large-scale flow cancel out at leading order. Indeed, if $\Psi(\boldsymbol{X})$ is the streamfunction of the small-scale current (taken independent of $\boldsymbol{x}$ for simplicity) and $Q(\boldsymbol{X}) = \nabla_{\boldsymbol{X}}^2 \Psi$ the associated vorticity, the contribution of the current to the solvability condition at $O(1)$ reads

$$\langle \boldsymbol{z} \cdot (\nabla\psi^{(1)} \times \nabla_{\boldsymbol{X}} Q + \nabla_{\boldsymbol{X}} \Psi \times \nabla\nabla_{\boldsymbol{X}}^2 \psi^{(1)}) \rangle$$

and is easily shown to vanish using integration by parts. Because of this cancellation, the effect of small-scale currents is smaller than that of a topography, and the scaling employed in studies of negative viscosity is different from the scaling employed here. In particular, the averaged equation obtained, for instance, by Gama *et al.* (1994) describes the evolution of the flow on a time scale slower than that considered here.

The multiple-scale analysis of § 3 is applied directly to the linearized quasi-geostrophic equation. It is therefore natural to ask how small the amplitude of the large-scale flow should be for the approach to be valid. We can answer this question and indicate what is the first non-trivial modification of our analysis that

https://doi.org/10.1017/S0022112099007430 Published online by Cambridge University Press

appears when nonlinear effects are taken into account. To do this, we scale the streamfunction (non-dimensionalized by $\mu^{-2}fL^2$) by an amplitude parameter $\delta \ll 1$, and reinstate the nonlinear term in (2.3). This term has the form $\delta\, \boldsymbol{z} \cdot (\nabla\psi \times \nabla\nabla^2\psi)$. With $\psi^{(0)} = \psi^{(0)}(\boldsymbol{x}, t)$, the largest nonlinear term appears at $O(\delta\epsilon^{-2})$ and is given by $\boldsymbol{z} \cdot [(\nabla\psi^0 + \nabla_{\boldsymbol{X}}\psi^{(1)}) \times \nabla_{\boldsymbol{X}}\nabla_{\boldsymbol{X}}^2\psi^{(1)}]$, whereas the largest nonlinear term with non-zero average appears at $O(\delta)$. (A cancellation similar to that discussed above is essential for this scaling.)

For $\delta \ll \epsilon$, the nonlinearity introduces no modification to the averaged equation (3.5), indicating that the linear theory is valid. Taking $\delta \sim \epsilon$ introduces the first non-trivial modification in § 3, with the appearance of the largest nonlinear term at $O(\epsilon^{-1})$ in equation (3.1) determining $\psi^{(1)}$. This equation becomes

$$\mathscr{A}\psi^{(1)} + \boldsymbol{z} \cdot [(\nabla\psi^0 + \nabla_{\boldsymbol{X}}\psi^{(1)}) \times \nabla_{\boldsymbol{X}}\nabla_{\boldsymbol{X}}^2\psi^{(1)}] = -\boldsymbol{z} \cdot (\nabla_{\boldsymbol{X}}\eta \times \nabla\psi^{(0)}). \tag{6.1}$$

Since it is nonlinear, there is no simple relationship between $\psi^{(1)}$ and $\psi^{(0)}$ similar to (3.2). Thus, although the $O(1)$ equation (3.4) remains formally the same (because the largest nonlinear term with non-zero average appears at $O(\epsilon)$ only), it does not provide a closed evolution equation for $\psi^{(0)}$. This is again in contrast with the situation encountered for large-scale flows superposed on small-scale currents where a weakly nonlinear evolution equation for the large-scale flow can be derived self-consistently (Gama *et al.* 1994). Here, such a self-consistent weakly nonlinear description cannot be obtained since a solution to the (fully) nonlinear equation (6.1) is needed to represent the first non-trivial effects of nonlinearity on the large-scale flow. It might be possible to model the relationship between $\psi^{(1)}$ and $\psi^{(0)}$ that emerges from (6.1) heuristically using a closure technique, e.g. based on statistical arguments (e.g. Merryfield & Holloway 1996), but we do not investigate this possibility further here.

The topography considered in this paper is characterized by a unique scale. This makes it possible to use a straightforward asymptotic technique to derive an averaged equation for the large-scale flow. It is, however, an extreme idealization which one may wish to relax. This could be done heuristically using renormalization-group (or coarse-graining) methods which can be regarded as equivalent to successive applications of the averaging technique employed here (e.g. Smith & Woodruff 1998; Avellaneda 1994). This should be relatively simple in the long-wave limit since in this case the averaging simply leads to a change (i.e. a renormalization) of the Ekman friction coefficient. The matter is more delicate in the short-wave limit because the averaging modifies the evolution equation drastically. Important effects associated with infra-red divergence can also be expected to be relevant in view of the typical spectrum of the ocean's bottom topography.

The averaging or homogenization approach employed here and the possible extensions just mentioned rely on a separation between the scales of the topography and of the leading-order motion. This scale-separation assumption, which is likely to hold only for a finite time (although a long one, of $O(\epsilon^{-1})$ at least), is the key to the implicit treatment of the interaction between flow and topography that is described by the averaged evolution equation. When it does not hold, (spatial) averaging cannot be employed and one has to consider explicitly the dynamics of the flow–topography interaction over a range of scales. This challenging problem requires the use of some closure technique and, generally, the treatment of the advective nonlinearity (see Holloway 1978). It has been considered by several authors using a variety of methods (e.g. Herring 1977; Holloway 1978; Frederiksen 1999; Alvarez & Tintoré 1998, and references therein); they notably conclude that the flow–topography interaction

https://doi.org/10.1017/S0022112099007430 Published online by Cambridge University Press

induces a force that drives the flow along topographic lines. Of course, such a force does not appear directly in our approach since it has the scale of the topography and hence is eliminated in the averaged evolution equation.

The author wishes to thank O. Bokhove and O. Bühler for helpful comments and discussions.

REFERENCES

Alvarez, A. & Tintoré, J. 1998 Topographic stress: importance and parameterization. In *Ocean Modeling and Parameterization* (ed. E. P. Chassignet & J. Verron). NATO Science Series, vol. 516, pp. 327–350. Kluwer.

Avellaneda, M. 1994 Homogenization and renormalization: the mathematics of multi-scale random media and turbulent diffusion. In *Dynamical Systems and Probabilistic Methods in Partial Differential Equations* (ed. P. Deift, C. D. Levermore & E. Wayne). Lectures in Applied Mathematics, vol. 31, pp. 251–268. AMS.

Bensoussan, A., Lions, J. L. & Papanicolaou, G. C. 1989 *Asymptotic Analysis of Periodic Structures.* Kluwer.

Frederiksen, J. S. 1999 Subgrid-scale parameterizations of eddy-topographic forces, eddy viscosity and stochastic flow over topography. *J. Atmos. Sci.* **56**, 1481–1494.

Gama, S., Vergassola, M. & Frisch, U. 1994 Negative eddy viscosity in isotropically forced two-dimensional flow: linear and nonlinear dynamics. *J. Fluid Mech.* **260**, 95–126.

Gurtin, M. E. & Pipkin, A. C. 1968 A general theory for heat conduction with finite wave speeds. *Arch. Rat. Mech. Anal.* **31**, 111–126.

Herring, J. R. 1977 Two-dimensional topographic turbulence. *J. Atmos. Sci.* **34**, 1731–1750.

Hinch, E. J. 1991 *Perturbation Methods*. Cambridge University Press.

Holloway, G. 1978 A spectral theory of nonlinear barotropic motion above irregular topography. *J. Phys. Oceanogr.* **8**, 414–427.

Kato, T. 1966 *Perturbation Theory for Linear Operators*. Springer.

Klyatskin, V. I. 1996 Localization of Rossby waves over a random cylindrical topography of the ocean bottom. *Izv. Atmos. Ocean. Phys.* **32**, 757–765.

Klyatskin, V. I., Gryanik, N. V. & Gurarie, D. 1998 Propagation and localization of Rossby waves over random topography (two-layer model). *Wave Motion* **28**, 333–352.

Merryfield, W. J. & Holloway, G. 1996 Inviscid quasi-geostrophic flow over topography: Testing statistical mechanical theory. *J. Fluid Mech.* **309**, 85–91.

Miller, R. K. 1978 An integro-differential equation for rigid heat conductors with memory. *J. Math. Anal. Appl.* **27**, 595–607.

Papanicolaou, G. C. 1995 Diffusion in random media. In *Surveys in Applied Mathematics* (ed. J. P. Keller), vol. 1, pp. 205–253. Plenum.

Pedlosky, J. 1987 *Geophysical Fluid Dynamics*. Springer.

Prahalad, Y. S. & Sengupta, D. 1986 Barotropic planetary waves on a random bottom. *Wave Motion* **8**, 407–414.

Reznik, G. M. & Tsybaneva, T. B. 1999 Planetary waves in a stratified ocean of variable depth. Part 1. Two-layer model. *J. Fluid Mech.* **388**, 115–145.

Rhines, P. B. 1970*a* Edge-, bottom-, and Rossby waves in a rotating stratified fluid. *Geophys. Fluid Dyn.* **1**, 273–302.

Rhines, P. B. 1970*b* Wave propagation in a periodic medium with application to the ocean. *Rev. Geophys.* **8**, 303–319.

Rhines, P. B. & Bretherton, F. 1973 Topographic Rossby waves in a rough-bottom ocean. *J. Fluid Mech.* **61**, 583–607.

Rosenbluth, M. N., Berk, H. L., Doxas, I. & Horton, W. 1987 Effective diffusion in laminar convective flows. *Phys. Fluids* **30**, 2636–2647.

Sengupta, D. 1994 Localization of Rossby over random topography: two-layer ocean. *J. Phys. Oceanogr.* **24**, 1065–1069.

Sengupta, D., Piterbarg, L. I. & Reznik, G. M. 1992 Localization of topographic Rossby waves over random relief. *Dyn. Atmos. Oceans* **17**, 1–21.

https://doi.org/10.1017/S0022112099007430 Published online by Cambridge University Press

Shraiman, B. I. 1987 Diffusive transport in a Rayleigh-Bénard convection cell. *Phys. Rev.* A **36**, 261–267.

Smith, L. M. & Woodruff, S. L. 1998 Renormalization-group analysis of turbulence. *Ann. Rev. Fluid Mech.* **30**, 275–310.

Thomson, R. E. 1975 The propagation of planetary waves over random topography. *J. Fluid Mech.* **70**, 267–285.

Vanneste, J. 2000 Rossby-wave frequency change induced by small-scale topography. *J. Phys. Oceanogr.* Submitted.

https://doi.org/10.1017/S0022112099007430 Published online by Cambridge University Press